Supporting Information

Dual Emissive Dinuclear Pt(II) Complexes and Application to Singlet Oxygen Generation

Marsel Z. Shafikov,*[a,b] Alfiya F. Suleymanova,[c] Roger J. Kutta,[a] Fabian Brandl,[a] Aleksander Gorski[d], Rafał Czerwieniec*[a]

[a]*Institut für Physikalische und Theoretische Chemie, Universität Regensburg, Universitätsstrasse 31, Regensburg, D-93053, Germany.*

[b]*Ural Federal University, Mira 19, Ekaterinburg, 620002, Russia.*

[c]*Chemistry Department, University of York, Heslington, York, YO10 5DD, UK*

[d]*Institute of Physical Chemistry, Polish Academy of Sciences, Kasprzaka 44/52, Warsaw, Poland*

Synthesis and chemical characterization.

General

NMR spectra were recorded on a Bruker AVANCE III HD 400 spectrometer, operating at 400 MHz for ^{1}H nuclei and at 376 MHz for ^{19}F nuclei, with residual protic solvent used as internal standard. Elemental analysis was carried out on an ELEMENTAR vario MICRO CUBE instrument at the central analytical services of the University of Regensburg. Mass-spectroscopy (FD-MS) was performed on a JEOL AccuTOF GCX instrument at the central analytical services of the University of Regensburg.

Synthetic procedures and characterizations

2,5-bis(5-(trifluoromethyl)pyridin-2-yl)thieno[3,2-b]thiophene (proligand **H_2L-1**). 2,5-bis(trimethylstannyl)thieno[3,2-b]thiophene (0.4 g, 0.860 mmol), 2-bromo-5-(trifluoromethyl)pyridine (0.388 g, 1.717 mmol) and dimethylformamide (50 mL) were put in a Schlenk flask which then was sealed with a rubber seal. The flask was then de-aerated by three-fold subsequent application of vacuum and argon lines. Then tetrakis(triphenylphosphine)palladium(0) 10 mol. % (0.1 g) was added quickly and the deaeration procedure was repeated. The flask was heated at 100°C in an oil bath for 12 hours and then cooled down to ambient temperature. The formed precipitated was filtered, washed with water and methanol subsequently, and dried under vacuum. Yield 55%. ^{1}H NMR ($CDCl_3$, 400 MHz): δH 8.84 (s, 2H), 7.95 (dd, 2H, J = 8.40, J=2.10 Hz), 7.91 (s, 2H), 7.81 (d, 2H, J=8.40). ^{19}F NMR ($CDCl_3$, 400 MHz): δF -62.87.

2,5-bis(5-(methyl)pyridin-2-yl)thieno[3,2-b]thiophene (proligand **H_2L-2**). 2,5-bis(trimethylstannyl)thieno[3,2-b]thiophene (0.5 g, 1.041 mmol), 2-bromo-5-methyl-pyridine (0.366 g,

2.082 mmol) and dimethylformamide (50 ml) were put in a Schlenk flask that then was sealed with a rubber seal. The flask was then de-aerated by three-fold subsequent application of vacuum and argon lines. Then tetrakis(triphenylphosphine)palladium(0) 10 mol. % (0.120 g) was added quickly and the deaeration procedure was repeated. The flask was heated at 100°C in an oil bath for 12 hours and then cooled down to ambient temperature. The formed precipitated was filtered, washed with water and methanol subsequently, and dried under vacuum affording the product at 68% yield. ^{1}H NMR ($CDCl_3$, 400 MHz): δH 8.41 (s, 2H), 7.73 (s, 2H), 7.60 (d, 2H, J = 8.10), 7.52 (dd, 2H, J=8.10, J=1.60), 2.36 (s, 6H).

Pt_2(dtfbp)(dpm)$_2$ (Complex **1**). The proligand **H_2L-1** (0.175 g, 0.407 mmol) was put in a flask with 50 mL of 2-ethoxyethanol under argon and heated to 120°C in an oil bath. Then K_2PtCl_4 (0.340 mg, 0.814 mmol) dissolved in 1 ml of water was added. Then the oil bath was let to cool down to 80°C and flask was heated for 48 hours with stirring. The flask was cooled to ambient temperature and the formed precipitate of dichlorobridged Pt(II) complex was filtered, washed with water and methanol successively, and dried under vacuum. To the dried dichloro-bridged Pt(II) complex in a flask with 50 mL of 2-ethoxyethanol was added (2,2,6,6-Tetramethyl-3,5-heptadionato)lithium (lithium dipivaloylmethanate - dpm) (0.790 g, 4.066 mmol). The flask was equipped with a condenser and heated at 100°C for 24 hours. The solvent then was removed in vacuo and 50 mL dichloromethane (dcm) was added. The precipitate was filtered and washed with 100 mL of dcm. The combined filtrate was collected, concentrated to 5 mL and used for column chromatography (silica gel, dcm) to give pure dinuclear Pt(II) complex **1** with 21% yield. ^{1}H NMR ($CDCl_3$, 400 MHz): δH 9.28 (s, 2H), 7.88 (dd, 2H, J = 8.60, J=1.90 Hz), 7.37 (d, 2H, J=8.40 Hz), 5.93 (s, 2H), 1.42 (s, 18H), 1.31(s, 18H). ^{19}F NMR ($CDCl_3$, 400 MHz): δF -63.04. FD-MS: calculated for $[M]^+$ ($C_{40}H_{44}F_6N_2O_4Pt_2S_2$) 1184.1930, found 1184.1545, Δ=0.0385. Elemental analysis: calculated C 40.54, H 3.74, N 2.36%; found C 40.59, H 3.62, N 2.18%.

Pt_2(dtbp)(dpm)$_2$ (Complex **2**). The proligand **H_2L-2** (0.140 g, 0.434 mmol) was put in a flask with 50 mL of 2-ethoxyethanol under argon and heated to 120°C in an oil bath. Then K_2PtCl_4 (0.368 mg, 0.868 mmol) dissolved in 1 mL of water was added. The oil bath was let to cool down to 80°C and flask was heated for 48 hours while stirring. The flask was cooled to ambient temperature and the formed precipitate of the dichlorobridged Pt(II) complex was filtered, washed with water and methanol successively, and dried under vacuum. To the dried dichloro-bridged Pt(II) complex in a flask with 50 ml of 2-ethoxyethanol was added (2,2,6,6-Tetramethyl-3,5-heptadionato)lithium (0.843 g, 4.342 mmol). The flask was equipped with a condenser and heated at 100°C for 24 hours. The solvent then was removed in vacuo and 50 mL dcm was added. The precipitate was filtered and washed with 100 mL dcm. The combined filtrate was collected, concentrated to 5 mL and used for column chromatography (silica gel, dcm) to give pure dinuclear Pt(II) complex **2** with 18% yield. ^{1}H NMR ($CDCl_3$, 400 MHz): δH 8.72 (s, 2H), 7.48 (dd, 2H, J = 8.35, J=1.50 Hz), 7.18 (d, 2H, J=8.10 Hz), 5.87 (s, 2H), 2.36 (s, 6H), 1.41 (s, 18H), 1.30 (s, 18H). FD-MS: calculated

for $[M]^+$ ($C_{40}H_{50}N_2O_4Pt_2S_2$) 1076.2495, found 1076.2603, Δ=0.0108. Elemental analysis: calculated C 44.60, H 4.68, N 2.60%; found C 44.74, H 4.56, N 2.34%.

Single crystal x-ray diffraction analysis

*Experimental for complex **1.*** Single clear orange needle-shaped crystals were obtained by convectional diffusion of methanol into a solution of complex **1** in dichloromethane. A suitable crystal with dimensions of 0.30×0.07×0.05 mm^3 was selected and mounted on a MITIGEN holder oil on a SuperNova, Single source at offset, Atlas diffractometer. The crystal was kept at stable *T* = 123.00(10) K during data collection. The structure was solved with the ShelXT[1] structure solution program using the Intrinsic Phasing solution method and by using Olex2[2] as the graphical interface. The model was refined with version 2016/6 of ShelXL[1] using Least Squares minimization.

*Experimental for complex **2.*** Single clear red plate-shaped crystals of **2** were obtained by convectional diffusion of methanol into a solution of complex **2** in chloroform. A suitable crystal of dimensions of 0.21×0.08×0.05 mm^3 was selected and mounted on a MITIGEN holder oil on a SuperNova, Single source at offset, Atlas diffractometer. The crystal was kept at a stable *T* = 123.01(10) K during data collection. The structure was solved with the ShelXT[1] structure solution program using the Intrinsic Phasing solution method and by using Olex2[2] as the graphical interface. The model was refined with version 2018/3 of ShelXL[1] using Least Squares minimization.

Table S1. Crystallographic data for complexes **1** and **2**

Crystallographic parameter	**1**	**2**
CCDC deposition number	1994515	1994516
Formula	$C_{40}H_{44}F_6N_2O_4Pt_2S_2$	$C_{41}H_{39}Cl_3F_6N_2O_4Pt_2S_2$
$D_{calc.}$/ g cm^{-3}	1.958	1.826
μ/mm^{-1}	14.419	15.005
Formula Weight	1185.07	657.93
Colour	clear orange	clear red
Shape	needle	plate
Size/mm^3	0.30×0.07×0.05	0.21×0.08×0.05
T/K	123.00(10)	123.01(10)
Crystal System	monoclinic	triclinic
Space Group	$P2_1/c$	P-1
a/Å	9.95761(15)	9.0918(3)
b/Å	9.68695(10)	9.1101(3)
c/Å	21.3470(3)	15.9150(4)
α/°	90	97.338(2)
β/°	102.5301(14)	99.050(2)
γ/°	90	110.350(3)
V/Å^3	2010.06(5)	1196.61(7)
Z	2	2
Z'	0.5	1
Wavelength/Å	1.54184	1.54184
Radiation type	CuK_α	CuK_α
Θ_{min}/°	4.243	5.282
Θ_{max}/°	73.566	74.094
Measured Refl.	21756	13650
Independent Refl.	3989	4692
Reflections Used	3949	4561
R_{int}	0.0219	0.0218
Parameters	316	297
Restraints	91	39
Largest Peak	1.223	0.739
Deepest Hole	-0.978	-0.913
GooF	1.100	1.049
wR_2 (all data)	0.0507	0.0443
wR_2	0.0506	0.0440
R_1 (all data)	0.0203	0.0186
R_1	0.0201	0.0179

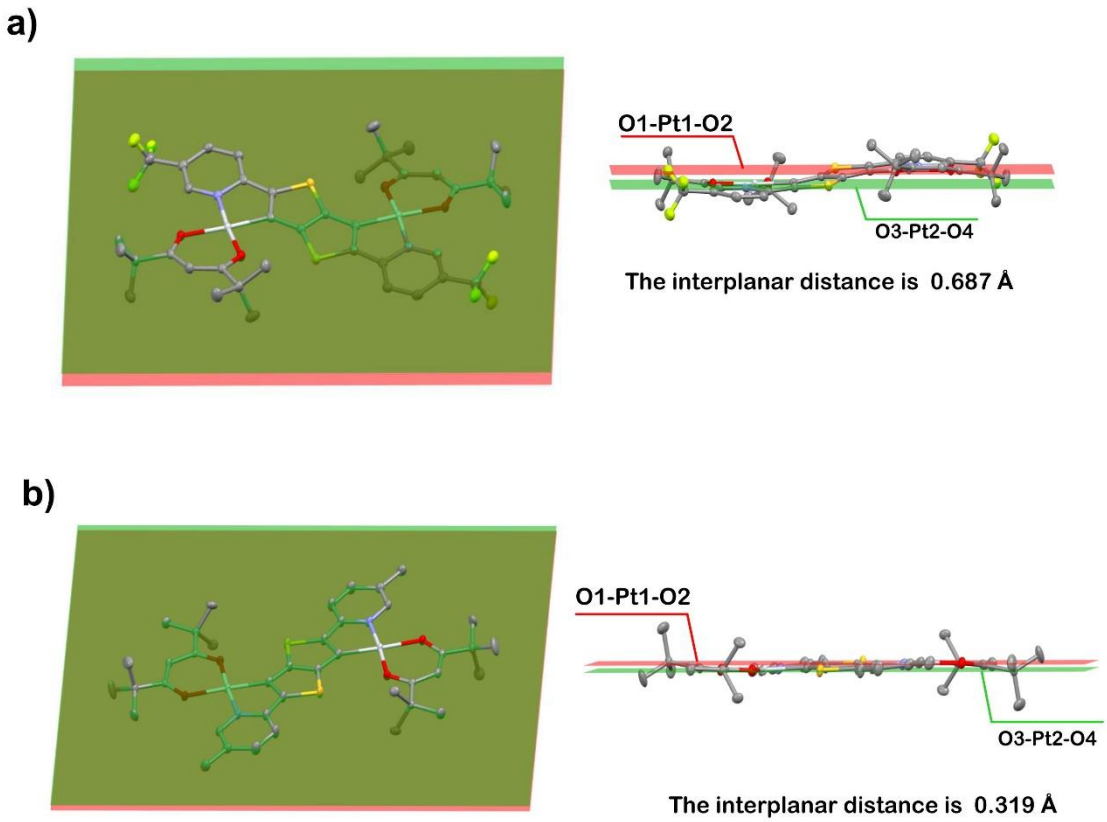

Figure S1. The XRD determined molecular geometries of complexes **1** (a) and **2** (b).

Optical spectroscopy. The steady state photophysical measurements were performed on solutions of complexes **1** and **2** in dcm. The UV-Vis absorption spectra were measured with a Varian Cary 300 double beam spectrometer. The emission room temperature photoluminescence spectra were measured with a Horiba Jobin Yvon DUETTA steady-state fluorescence spectrometer. The excitation spectra were measured with a Horiba Jobin Yvon Fluorolog-3 steady-state fluorescence spectrometer. The emission decay times were measured with a PicoBright PB-375 pulsed diode laser (λ_{exc} = 378 nm, pulse width 100 ps) used as the excitation source, and the PL signal was detected with a cooled photomultiplier attached to a FAST ComTec multichannel scalar PCI card with a time resolution of 250 ps. The PL quantum yield was determined with a Hamamatsu C9920-02 system equipped with a Spectralon® integrating sphere with the measurement error of 1% under ambient conditions.

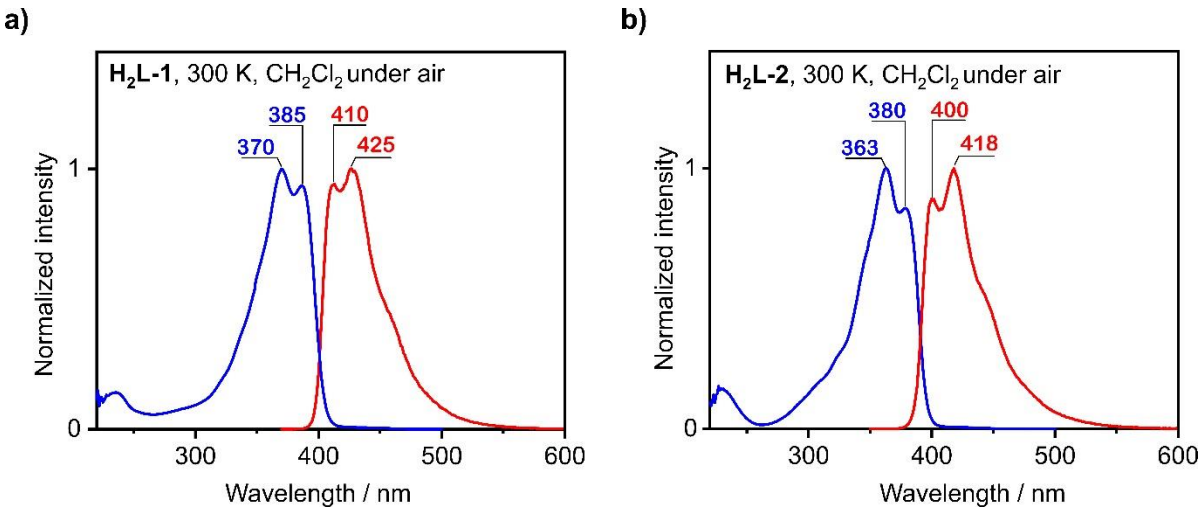

Figure S2. Absorption (blue) and emission (red) spectra of proligand **H_2L-1** (a), and of proligand **H_2L-2** (b), recorded in dcm solution under ambient conditions.

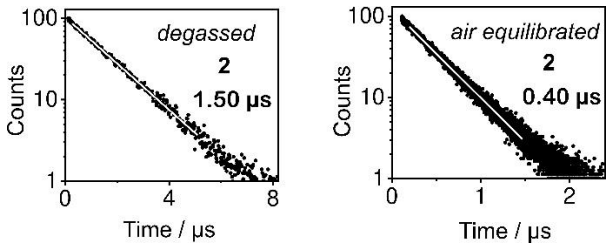

Figure S3. Emission decay profiles of **2** in CH_2Cl_2 ($c \approx 10^{-5}$ M) measured at room temperature under degassed and air-equilibrated conditions as indicated in the insets.

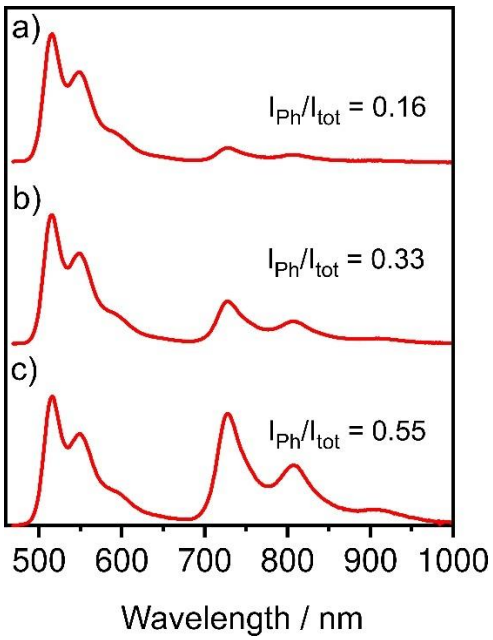

Figure S4. The emission spectra of complex **2** in diluted dcm solution at room temperature: (a) air equilibrated solution, λ_{exc} = 460 nm; (b) degassed solution, λ_{exc} = 460 nm; (c) degassed solution, λ_{exc} = 390 nm.

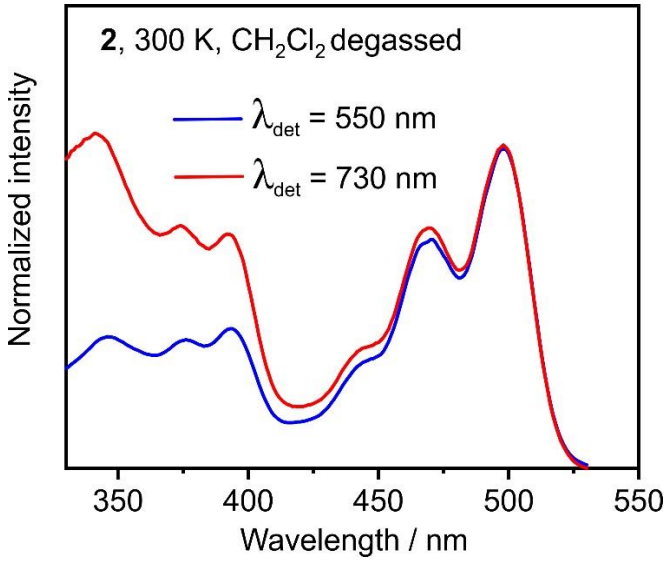

Figure S5 Excitation spectra measured for degassed CH_2Cl_2 solution of complex **2** with detection at λ_{det} = 550 nm (blue trace) and λ_{det} = 730 nm (red trace).

Sub-ps Pump/Supercontinuum-Probe Spectroscopy. The femtosecond transient absorption apparatus is based on the design published earlier[3]. A Ti:Sapphire oscillator-regenerative amplifier laser system (Coherent Libra) generates 100 fs pulses with 1.0 mJ energy at 1 kHz repetition rate. With 0.67 mJ of these pulses a collinear parametric amplifier (TOPAS-C, Light Conversion) was pumped. The output of

the TOPAS was compressed with a pair of quartz prisms, and used to excite the sample at into the $S_1 \leftarrow S_0$ absorption band, i.e. λ_{exc} = 530 nm for complex **1** and λ_{exc} = 500 nm for complex **2**. In each case the with pulse energy was set to ca. 300 nJ focused to ca. 100 μm.

The remaining 0.33 mJ of the Ti:Sa output drive a two stage NOPA[4] which produces ca. 20 μJ pulses at 510 nm. These were compressed with a quartz prism pair and focused onto a 1 mm thick CaF_2 plate in order to generate a white-light supercontinuum for the probe beam. The plate was mounted on a XY stage and moved continuously. The white light supercontinuum was spectrally filtered and split into a reference and signal beam path. At the sample position the spot size of the probe pulse was ca. 60 μm. The signal and reference beams were imaged onto entrance slits of two home-build grating spectrographs and recorded with photodiode arrays (Hamamatsu, S3901-512Q, 512 pixels) at 1.5 nm resolution. The time delay between probe and pump is controlled via variation of the probe beam path using a delay stage (Physik Instrumente M-531.2S) equipped with an open corner cube reflector.

The sample solution was pumped continuously through a self-made quartz cell. Each scan was performed from -0.36 ps to 1.0 ps in 6 fs steps, and from 1 ps to 1.8 ns in 240 steps with logarithmic temporal spacing. At each delay position of a scan an average over typically 100 transient absorption spectra were taken, each calculated for a baseline-corrected single shot. Averaging of at least eight independent scans result in the final spectra for either parallel $\Delta A_{\parallel}$ and perpendicular $\Delta A_{\perp}$ polarization with respect to the angles between pump and probe pulse polarization, which was set via a λ/2 plate in the pump beam path. The averaged pre-t_0 laser scatter signal was subtracted from the data and the ca. 1.5 ps chirp of the white light was corrected for prior to data analysis using the coherent artefact as an indicator for time zero at each wavelength. Spectra under magic angle polarization were calculated via Equation 1.

$$\Delta A_M = \frac{(2\Delta A_{\perp} + \Delta A_{\parallel})}{3} \quad (1)$$

No smoothing or filtering procedures were applied to the data. The raw data shown in Figure S6.

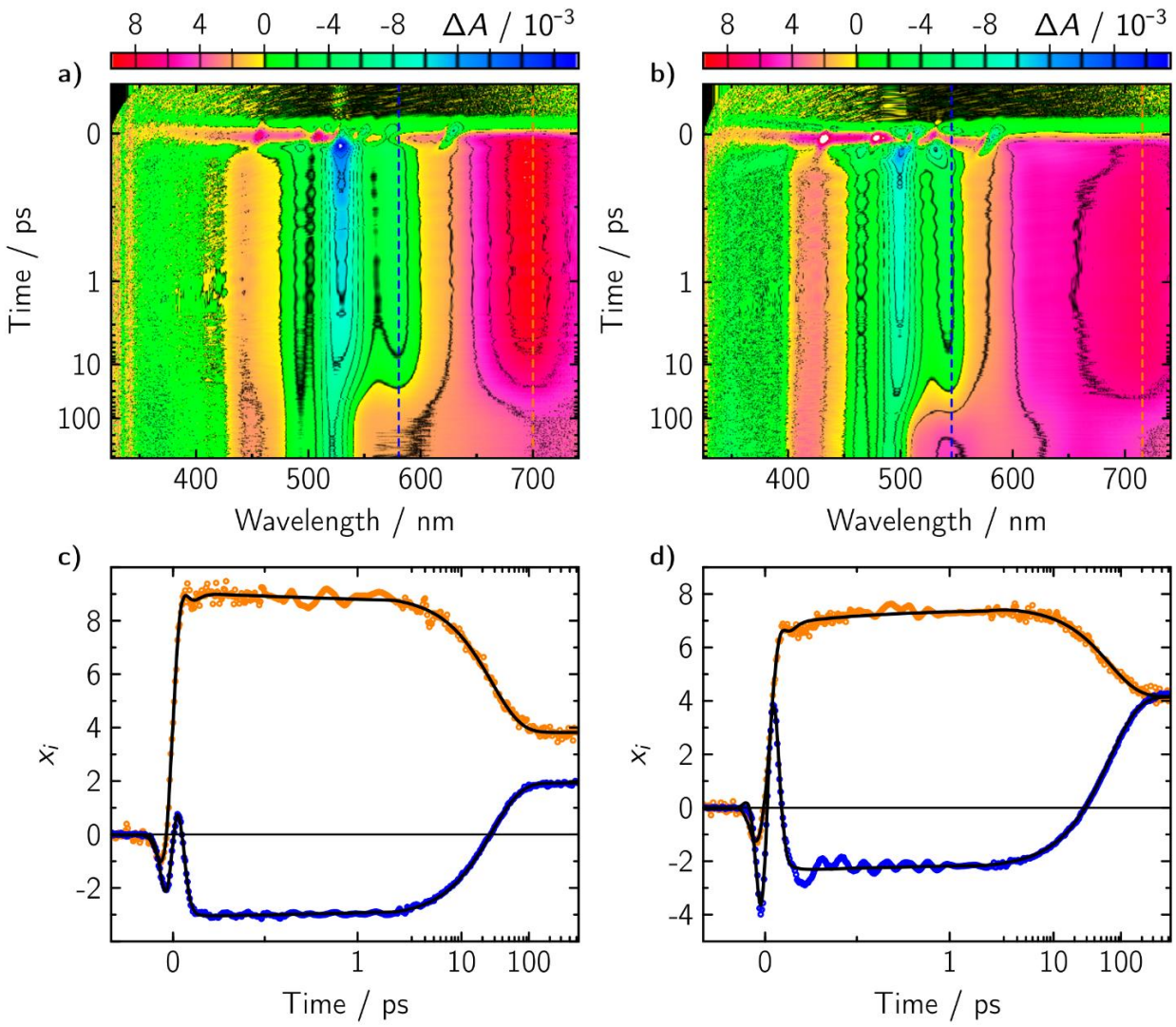

Figure S6. Transient absorption spectra in false color representation of complex **1** (**a**) and **2** (**b**) in dcm when exciting into the corresponding $S_1 \leftarrow S_0$ transition. **c** and **d** show two selected time traces each along a certain probe wavelength as indicated by a dashed line in **a** and **b**, respectively. The black solid lines in **c** and **d** show the corresponding global fit to the data.

Transient absorption data analysis and modelling. Global fitting was performed using an in-house written program described previously.[5,6] Transient absorption data consist of a series of difference spectra recorded at a number of delay times, ΔA(t,λ), which may be represented as a rectangular matrix ΔA of dimension $N_T \times N_L$. In this matrix each column is a time trace for a fixed wavelength of N_T points, and each row is a spectrum at a given delay time of N_L points. This matrix can be decomposed into a sum of products of one-dimensional functions by a global fit. Here, the assumption is made that the data can be modelled by a linear combination of products between spectra, $S_k(\lambda)$, and concentration-time profiles, $c_k(t)$, according to Eq. 2.

$$\Delta A_{ij} = \sum_{k=1}^{N} c_k(t_i) S_k(\lambda_j) = \sum_{k=1}^{N} c_{ik} S_{jk} \qquad (2)$$

In Eq. 2 ΔA_{ij} can be approximated by matrix $\mathbf{D}$, in which the time profiles are represented as a linear combination of known analytic functions, $f_k(t)$:

$$D_{ij} = \sum_{k=1}^{N_C} c_k(t_i) S_k(\lambda_j) \tag{3}$$

$$c_k(t) = \sum_{k=1}^{N_F} f_l(t) X_{lk} \tag{4}$$

where N_C is the number of distinct spectral species and N_F is the number of analytic time functions. The model data matrix **D** can be written as

$$\mathbf{D} = \mathbf{CS} = \mathbf{FXS} = \mathbf{FB} \tag{5}$$

where **C** is defined as a $N_T \times N_C$ matrix with elements, $C_{ik} = c_k(t_i)$, and F is defined as a $N_T \times N_C$ matrix with elements, $F_{il} = f_l(t_i)$. Thus, the *k*-th row of the matrix $\mathbf{B}$, with elements $B_{kj} = b_k(\lambda_j)$, corresponds to the spectral changes associated with the time function, $f_k(t)$. When using exponential decays (convoluted with the instrument response) as analytical function the corresponding spectra are called decay associated difference spectra (DADS). The linear least squares problem

$$\chi^2 = \|\Delta\mathbf{A} - \mathbf{FB}\|^2 = \mathrm{Min} \tag{6}$$

for given matrices $\mathbf{\Delta A}$ and $\mathbf{F}$ can be solved by efficient existing algorithms. A nonlinear least squares algorithm is used for further optimization of χ^2 by optimizing the rate constants in $\mathbf{F}$, so that the DADS and the corresponding rate constants are the unique result of the global fit not requiring any model for the kinetics involved in the transient processes. The details of a model will be entirely defined in the matrix $\mathbf{X}$ that relates the actual species kinetics to the elementary function, $f_k(t)$. The appropriate matrix, $\mathbf{X}$, can be chosen depending on the model and the species associated spectra (SAS) in matrix $\mathbf{S}$ are calculated according to Eq. 7.

$$\mathbf{S} = \mathbf{X}^{-1}\mathbf{B} \tag{7}$$

The χ^2 value found in the global fit does not change by this step and, thus, this procedure has the advantage that all interpretation is performed with the same quality of fit.

General kinetic model.

The analytic fitting function shown in Eq. 8 was used in the global lifetime analysis in order to determine the dynamics of each complex

$$f_k(\mathrm{t}) = \sum_{i=0}^{2} \frac{\mathrm{d}^i}{\mathrm{d}t^i} g_{\mathrm{art}}(t - t_0) + \left(\delta(t) + \sum_{j=1}^{N} \exp(-\kappa_k t) \right) \otimes g_{\mathrm{app}}(t - t_0) \tag{8}$$

where $\otimes\, g_{\mathrm{app}}(t - t_0)$ indicates convolution with the apparatus function approximated by a Gaussian, $\delta(t)$ is the Dirac delta function, $\sum_{i=0}^{2} \frac{\mathrm{d}^i}{\mathrm{d}t^i} g_{\mathrm{art}}(t - t_0)$ are a Gaussian and its first and second derivatives with identical temporal widths as the apparatus function allowing to account for the coherent artefact, and N is the number of exponentials describing the dynamics of the TA change over time. The general photophysical processes can be described with the differential equations of Eq. 9.

$$\frac{\mathrm{d}}{\mathrm{d}t}\begin{pmatrix}[\,\mathrm{S}_1\,]\\ [\,\mathrm{T}_1\,]\end{pmatrix} = -\begin{pmatrix}k_{\mathrm{ic}} + k_{\mathrm{r}} + k_{\mathrm{isc}} & 0\\ -k_{\mathrm{isc}} & k_{\mathrm{bisc}}\end{pmatrix}\begin{pmatrix}[\,\mathrm{S}_1\,]\\ [\,\mathrm{T}_1\,]\end{pmatrix} \tag{9}$$

The eigenvalues of the rate constant matrix are given in Eq. 10 to 11 and are absolutely determined by the global fit described above.

$$\kappa_1 = k_{\text{ic}} + k_{\text{r}} + k_{\text{isc}} \quad (10)$$

$$\kappa_2 = k_{\text{bisc}} \quad (11)$$

In this simple model one obtains the following relationship between the species associated spectra, SAS_i, and the DADS, D_i, c_0 is the contribution of the ground state spectrum, SAS_{S_0}, and Φ_{T_1} is the triplet state quantum yield:

$$\text{SAS}_{\text{S}_1} = \frac{(\text{D}_1 + \text{D}_2)}{c_0} + \text{SAS}_{\text{S}_0} \quad (12)$$

$$\text{SAS}_{\text{T}_1} = \frac{(\kappa_1 - \kappa_2)\text{D}_2}{c_0 \Phi_{\text{T}_1} \kappa_1} + \text{SAS}_{\text{S}_0} \quad (13)$$

Here, c_0 and Φ_{T_1} are the only undetermined parameters. However, one can at least find upper or lower bounds by the requirement that the resulting SAS must be positive, and should not show any of the characteristic bands of the other species. In particular the negative peaks from the ground state bleach should disappear in the SAS. The determination of the individual parameters for each individual case is shown in Figures S7 and S8.

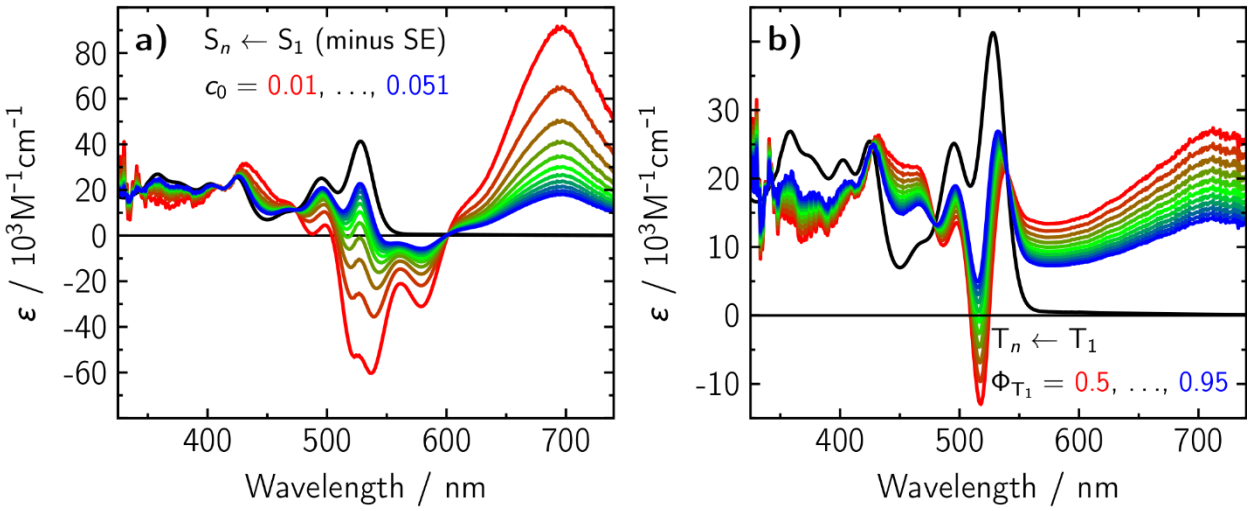

Figure S7. SAS of complex **1** in di-chlormethane in the S_1 state, $S_n \leftarrow S_1$ transitions (minus stimulated emission (SE)), (**a**), and in the T_1 state, $T_n \leftarrow T_1$ transitions, (**b**). The contribution of the ground state spectrum, c_0, was varied between 0.01 (red) and 0.051 (blue). Below $c_0 = 0.03$ the S_1 spectrum becomes negative and above contributions of the S_0 spectrum arise. The triplet yield, Φ_{T_1}, was varied between 0.5 (red) and 0.95 (blue). The lower bound for Φ_{T_1} is 0.75 since below this value the T_1 spectrum becomes negative. Above $\Phi_{T_1} = 0.95$ the signatures of the S_0 spectrum start to arise. Thus, the preferred value of Φ_{T_1} is ca. 0.85. The S_0 spectrum is also plotted in both panels for comparison.

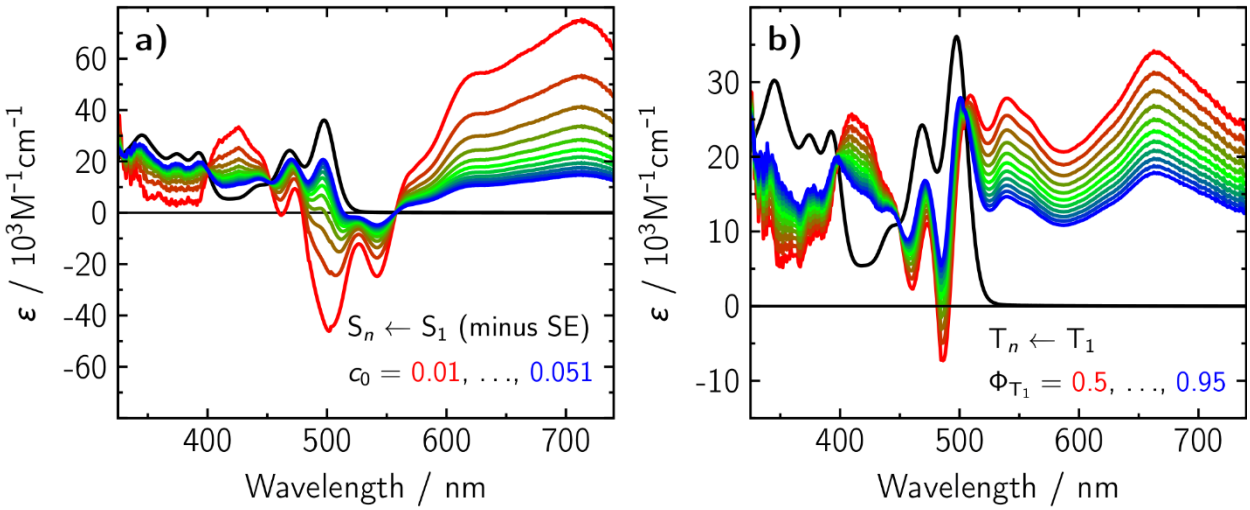

Figure S8. SAS of complex **2** in di-chlormethane in the S_1 state, $S_n \leftarrow S_1$ transitions (minus stimulated emission (SE)), (**a**), and in the T_1 state, $T_n \leftarrow T_1$ transitions, (**b**). The contribution of the ground state spectrum, c_0, was varied between 0.01 (red) and 0.051 (blue). Below $c_0 = 0.03$ the S_1 spectrum becomes negative and above contributions of the S_0 spectrum arise. The triplet yield, Φ_{T_1}, was varied between 0.5 (red) and 0.95 (blue). The lower bound for Φ_{T_1} is 0.7 since below this value the T_1 spectrum becomes negative. Above $\Phi_{T_1} = 0.9$ the signatures of the S_0 spectrum start to arise. Thus, the preferred value of Φ_{T_1} is ca. 0.8. The S_0 spectrum is also plotted in both panels for comparison.

Singlet Oxygen Generation Studies

Measurements of quantum efficiencies (ϕ_Δ) of singlet oxygen generation ($^1O_2$ ($^1\Delta_g$) emission at λ_{max} = 1275 nm) have been performed with a custom built highly sensitive experimental setup based on a BENTHAM DTMc300 Double Monochromator equipped with a TE Cooled PMT (Hamamatsu H10330C-75, 950–1700 nm registration range). A 405 nm continuous laser was used as photoexcitation source. The singlet oxygen quantum yield was determined by the relative method[7]. The efficiencies ϕ_Δ were determined with respect to the well-known standard phenalenone (ϕ_Δ = 0.96 in dcm at ambient temperature).[8] The accuracy in the estimation of singlet oxygen emission quantum yield was ±10%.

Computations. All calculations were carried out with the Gaussian 09 package[9] utilizing the DFT approach with the M11L functional[10,11] and the def2-SVP basis set[12] including ECPs for the Pt(II) ion. Geometry optimizations were conducted with the "tight" criteria. The C-PCM solvation model[13] was applied with solvent parameters for dcm.

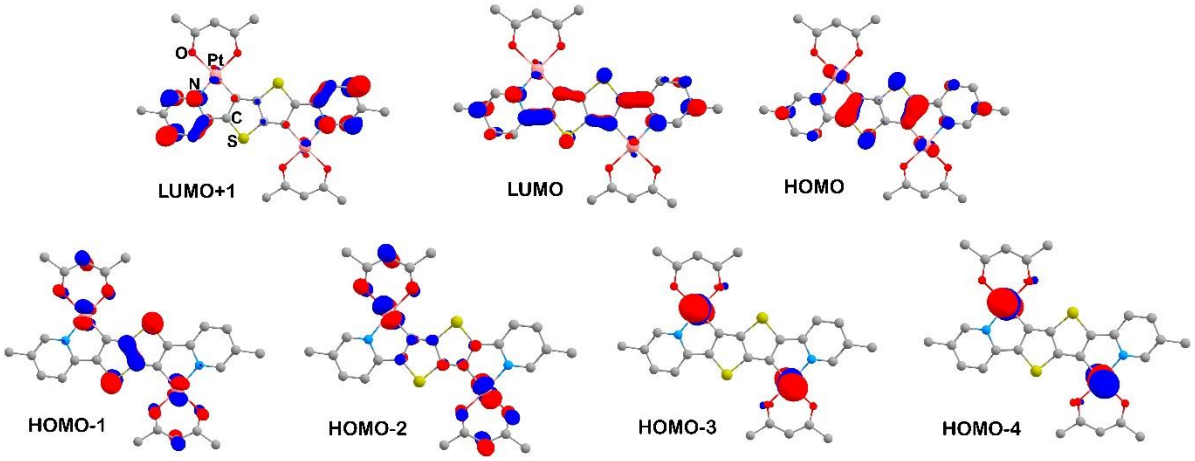

Figure S9. Iso-surface contour plots (isovalue = 0.05) of the several frontier molecular orbitals calculated for model complex **2'** in the relaxed T_1 state geometry.

Table S2. The key structural parameters of complex **1** derived from the single crystal XRD experiment and DFT optimized ground state (S_0) and T_1 state geometries of model complex **1'**. The atom numbering corresponds to that given in Figure 1a.

Parameter	XRD (esd)	Ground state (S_0)	Emitting state (T_1)
Bonds (Å)			
Pt1-C1	1.959(3)	1.965	1.952
Pt1-N1	2.002(3)	2.019	2.016
Pt1-O1	2.053(2)	2.062	2.062
Pt1-O2	1.999(2)	1.988	1.993
Angles (degree^o)			
C1-Pt1-N1	81.29(12)	80.593	81.633
O1-Pt1-O2	92.63(9)	91.651	91.829
C1-Pt1-O1	172.67(10)	175.148	175.735
C1-Pt1-O2	94.30(11)	93.139	92.377
N1-Pt1-O1	91.97(10)	94.619	94.164
N1-Pt1-O2	173.93(10)	173.730	174.004
Torsion angles (degree^o)			
C3-N1-Pt1-O1	175.4(2)	178.955	178.984
C2-C1-Pt1-O2	169.6(2)	179.664	179.742
C1-C2-C3-N1	1.8(4)	0.359	0.450

Table S3. The key structural parameters of complex **2** derived from the single crystal XRD experiment and DFT optimized ground state (S_0) and T_1 state geometries of model complex **2'**. The atom numbering corresponds to that given in Figure 1b.

Parameter	XRD (esd)	Ground state (S_0)	Emitting state (T_1)
Bonds (Å)			
Pt1-C1	1.968(3)	1.968	1.956
Pt1-N1	2.005(3)	2.020	2.014
Pt1-O1	2.0497(2)	2.069	2.069
Pt1-O2	1.9983(17)	1.993	1.997
Angles (degree^o)			
C1-Pt1-N1	81.26(10)	80.668	81.595
O1-Pt1-O2	92.26(7)	91.337	91.506
C1-Pt1-O1	172.6(1)	175.443	175.905
C1-Pt1-O2	94.44(9)	93.220	92.589
N1-Pt1-O1	91.99(8)	94.775	94.310
N1-Pt1-O2	175.61(9)	173.889	174.185
Torsion angles (degree^o)			
C3-N1-Pt1-O1	173.4(2)	179.989	180.000
C2-C1-Pt1-O2	175.9(2)	179.995	180.000
C1-C2-C3-N1	0.4(4)	0.002	0.000

Table S4. DFT calculated frontier orbital energies and atomic contributions of complex **1'** in the T_1 state geometry resulting from Mulliken population analysis.

Orbital	**Energy, eV**	**Contribution, % (Mulliken)**				
		Pt1	**acac1**	**dtfbp**	**Pt2**	**acac2**
LUMO+4	-2.103	2	44	8	2	44
LUMO+3	-2.199	1	32	34	1	32
LUMO+2	-2.440	1	5	88	1	5
LUMO+1	-2.672	3	1	92	1	3
LUMO	-3.587	3	0	94	0	3
HOMO	-5.222	7	1	84	7	1
HOMO-1	-5.871	17	22	22	17	22
HOMO-2	-5.896	14	21	30	14	21
HOMO-3	-5.952	45	2	6	45	2
HOMO-4	-5.985	46	3	4	46	3

dtfbp – dithiophenebipyridine
acac – acetylacetonate

Table S5. DFT calculated frontier orbital energies and atomic contributions of complex **12'** in the T_1 state geometry resulting from Mulliken population analysis.

Orbital	Energy, eV	Contribution, % (Mulliken)				
		Pt1	**acac1**	**dtbp**	**Pt2**	**acac2**
LUMO+4	-1.959	2	27	42	2	27
LUMO+3	-2.048	1	45	8	1	45
LUMO+2	-2.157	0	22	56	0	22
LUMO+1	-2.342	3	2	90	3	2
LUMO	-3.169	3	0	94	3	0
HOMO	-4.882	5	1	88	5	1
HOMO-1	-5.693	13	13	48	13	13
HOMO-2	-5.698	19	16	30	19	16
HOMO-3	-5.802	45	2	6	45	2
HOMO-4	-5.836	46	2	4	46	2

dtbp – dithiophenebipyridine
acac – acetylacetonate

Table S6. TD-DFT calculated lowest triplet and singlet states of **1'** in the T_1 state geometry

State, energy (eV)	*f* (oscillator strength)	Contributing transition coefficients*	Character**
triplets			
T_1, 1.449	(triplet)	HOMO→LUMO (0.71)	$LC^{dtfbp}/M^{Pt}L^{dtfbp}CT$
T_2, 2.204	(triplet)	HOMO–1→LUMO (0.69) HOMO→LUMO+1 (0.10)	$M^{Pt}L^{dtfbp}CT/L^{acac}L^{dtfbp}CT/LC^{dtfbp}$
T_3, 2.211	(triplet)	HOMO–2→LUMO (0.69) HOMO–6→LUMO (0.11)	$M^{Pt}L^{dtfbp}CT/\ L^{acac}L^{dtfbp}CT/\ LC^{dtfbp}$
T_4, 2.330	(triplet)	HOMO–3→LUMO (0.71)	$M^{Pt}L^{dtfbp}CT$
T_5, 2.362	(triplet)	HOMO–4→LUMO (0.71)	$M^{Pt}L^{dtfbp}CT$
singlets			
S_1, 2.020	0.4095	HOMO→LUMO (0.69)	$LC^{dtfbp}/M^{Pt}L^{dtfbp}CT$
S_2, 2.357	0.0000	HOMO–3→LUMO (0.71)	$M^{Pt}L^{dtfbp}CT$
S_3, 2.383	0.0000	HOMO–1→LUMO (0.69) HOMO→LUMO+1 (0.12)	$M^{Pt}L^{dtfbp}CT/L^{acac}L^{dtfbp}CT/LC^{dtfbp}$
S_4, 2.389	0.0030	HOMO–4→LUMO (0.71)	$M^{Pt}L^{dtfbp}CT$
S_5, 2.415	0.1615	HOMO–2→LUMO (0.67) HOMO–6→LUMO (0.20)	$M^{Pt}L^{dtfbp}CT/\ L^{acac}L^{dtfbp}CT/\ LC^{dtfbp}$

*Square of the coefficient multiplied by two gives percentage contribution of the transition to formation of the excited state.

**MLCT – Metal (M) to Ligand (L) Charge Transfer. LC-Ligand Centered. LLCT – Ligand to Ligand Charge Transfer.

Table S7. TD-DFT calculated lowest triplet and singlet states of **2'** in the T_1 state geometry

State, energy (eV)	*f* (oscillator strength)	Contributing transition coefficients*	Character**
triplets			
T_1, 1.494	(triplet)	HOMO→LUMO (0.71)	$LC^{dtbp}/M^{Pt}L^{dtbp}CT$
T_2, 2.390	(triplet)	HOMO–2→LUMO (0.53) HOMO→LUMO+1 (-0.43) HOMO–5→LUMO (0.14)	$M^{Pt}L^{dtbp}CT/ LC^{dtbp} /L^{acac}L^{dtbp}CT$
T_3, 2.396	(triplet)	HOMO–1→LUMO (0.69) HOMO–6→LUMO (0.10)	$LC^{dtbp} /L^{acac}L^{dtbp}CT / M^{Pt}L^{dtbp}CT$
T_4, 2.483	(triplet)	HOMO–2→LUMO (0.44) HOMO→LUMO+1 (0.55)	$LC^{dtbp}/M^{Pt}L^{dtbp}CT/L^{acac}L^{dtbp}CT$
T_5, 2.600	(triplet)	HOMO–3→LUMO (0.71)	$M^{Pt}L^{dtbp}CT$
singlets			
S_1, 2.125	0.6108	HOMO→LUMO (0.69)	$LC^{dtbp}/M^{Pt}L^{dtbp}CT$
S_2, 2.588	0.0000	HOMO–2→LUMO (0.49) HOMO→LUMO+1 (0.51)	$M^{Pt}L^{dtbp}CT/ LC^{dtbp} /L^{acac}L^{dtbp}CT$
S_3, 2.628	0.0000	HOMO–3→LUMO (0.70)	$M^{Pt}L^{dtbp}CT$
S_4, 2.661	0.0039	HOMO–4→LUMO (0.71)	$M^{Pt}L^{dtbp}CT$
S_5, 3.667	0.1835	HOMO–1→LUMO (0.65) HOMO–6→LUMO (0.25) HOMO→LUMO+2 (-0.12)	$LC^{dtbp} /L^{acac}L^{dtbp}CT / M^{Pt}L^{dtbp}CT$

*Square of the coefficient multiplied by two gives percentage contribution of the transition to formation of the excited state.

**MLCT – Metal (M) to Ligand (L) Charge Transfer. LC-Ligand Centered. LLCT – Ligand to Ligand Charge Transfer.

Table S8. DFT optimized ground state (S_0) and T_1 state geometry of **1'** in cartesian (XYZ) coordinates

State S_0				**State T_1**			
Pt	3.527330000	-1.133632000	-0.009618000	Pt	3.509017000	-1.135791000	-0.015616000
O	2.681132000	-2.933007000	-0.025979000	O	2.651934000	-2.935143000	-0.032109000
O	5.416602000	-1.957461000	0.066151000	O	5.396187000	-1.962567000	0.067674000
C	1.906271000	1.185359000	-0.053834000	C	1.912121000	1.206206000	-0.065847000
C	1.798030000	-0.201187000	-0.057059000	C	1.783750000	-0.223834000	-0.069099000
C	0.440379000	-0.547037000	-0.067678000	C	0.448056000	-0.547831000	-0.082292000
C	-0.440036000	0.548338000	-0.067911000	C	-0.448056000	0.547829000	-0.082293000
S	0.401348000	2.048093000	-0.061840000	S	0.418690000	2.060098000	-0.077742000
C	-1.797733000	0.202370000	-0.061565000	C	-1.783750000	0.223832000	-0.069096000
C	-1.905759000	-1.184198000	-0.061062000	C	-1.912122000	-1.206208000	-0.065839000
S	-0.400825000	-2.046844000	-0.066761000	S	-0.418690000	-2.060100000	-0.077735000
C	3.216799000	1.734903000	-0.031517000	C	3.210521000	1.738481000	-0.041086000
C	-3.216109000	-1.734255000	-0.042487000	C	-3.210522000	-1.738482000	-0.041074000
N	-4.181749000	-0.776547000	-0.019872000	N	-4.181420000	-0.764259000	-0.013384000
C	-5.458311000	-1.121690000	-0.001536000	C	-5.455129000	-1.106690000	0.013594000
C	-5.864449000	-2.442607000	-0.004293000	C	-5.870362000	-2.426147000	0.015360000
C	-3.567091000	-3.086850000	-0.046117000	C	-3.578168000	-3.095434000	-0.039962000
C	-4.893921000	-3.443166000	-0.026714000	C	-4.901108000	-3.442444000	-0.012480000
C	3.568517000	3.087360000	-0.030989000	C	3.578166000	3.095433000	-0.039981000
C	4.895455000	3.443029000	-0.007959000	C	4.901106000	3.442444000	-0.012490000
C	5.865487000	2.441870000	0.015591000	C	5.870359000	2.426148000	0.015366000
C	5.458607000	1.121240000	0.015431000	C	5.455128000	1.106691000	0.013596000
N	4.181918000	0.776753000	-0.006991000	N	4.181419000	0.764258000	-0.013390000
C	-7.313414000	-2.798392000	0.035036000	C	-7.316771000	-2.774153000	0.041979000
C	7.315179000	2.796943000	0.024515000	C	7.316768000	2.774156000	0.041985000
H	-6.179673000	-0.291388000	0.015061000	H	-6.175266000	-0.275240000	0.036599000
H	-2.778555000	-3.849913000	-0.067044000	H	-2.794726000	-3.864428000	-0.061838000
H	2.780342000	3.850877000	-0.048747000	H	2.794724000	3.864426000	-0.061873000
H	6.179394000	0.290576000	0.036701000	H	6.175265000	0.275240000	0.036605000
Pt	-3.527663000	1.134061000	-0.016682000	Pt	-3.509017000	1.135790000	-0.015617000
O	-5.417530000	1.956461000	0.057450000	O	-5.396186000	1.962569000	0.067670000
O	-2.682244000	2.933787000	-0.023382000	O	-2.651932000	2.935142000	-0.032120000
C	-3.298271000	4.031307000	0.013963000	C	-3.265930000	4.033211000	0.006444000
C	-4.683584000	4.200743000	0.064520000	C	-4.651201000	4.204871000	0.064872000
C	-5.652413000	3.186104000	0.084055000	C	-5.623697000	3.194336000	0.092292000
C	-2.411967000	5.225247000	0.000352000	C	-2.379108000	5.226474000	-0.015509000
C	-7.090944000	3.563831000	0.143053000	C	-7.059803000	3.578585000	0.158062000
C	3.296521000	-4.031033000	0.006466000	C	3.265933000	-4.033212000	0.006441000
C	4.681647000	-4.201427000	0.058870000	C	4.651205000	-4.204871000	0.064865000
C	5.650871000	-3.187341000	0.086389000	C	5.623699000	-3.194335000	0.092291000
C	7.089092000	-3.566043000	0.146797000	C	7.059806000	-3.578582000	0.158062000
C	2.409650000	-5.224426000	-0.015611000	C	2.379113000	-5.226476000	-0.015523000
H	-5.049531000	5.233570000	0.092241000	H	-5.014362000	5.238626000	0.092038000
H	-1.785186000	5.211831000	-0.909269000	H	-1.759140000	5.210993000	-0.929702000
H	-1.713433000	5.178135000	0.854919000	H	-1.674546000	5.180018000	0.834061000
H	-2.962562000	6.176657000	0.040625000	H	-2.928732000	6.178269000	0.027178000
H	-7.256642000	4.651206000	0.159051000	H	-7.220871000	4.666607000	0.172129000
H	-7.554470000	3.118330000	1.041180000	H	-7.519998000	3.136814000	1.059710000
H	-7.624217000	3.132468000	-0.722550000	H	-7.599254000	3.146712000	-0.703423000
H	5.047047000	-5.234573000	0.081447000	H	5.014367000	-5.238625000	0.092026000
H	7.625134000	-3.128158000	-0.713790000	H	7.599245000	-3.146754000	-0.703454000
H	7.254372000	-4.653569000	0.154996000	H	7.220873000	-4.666603000	0.172179000
H	7.549978000	-3.127673000	1.049786000	H	7.520015000	-3.136765000	1.059680000
H	1.783970000	-5.205074000	-0.925882000	H	1.759159000	-5.210996000	-0.929725000
H	1.710131000	-5.182265000	0.838415000	H	1.674538000	-5.180020000	0.834036000
H	2.959741000	-6.176329000	0.019490000	H	2.928738000	-6.178271000	0.027171000

H	-5.183492000	-4.503039000	-0.033106000	H	-5.199451000	-4.499576000	-0.010989000
H	5.185049000	4.502980000	-0.005427000	H	5.199449000	4.499576000	-0.011002000
F	-8.077888000	-1.748515000	-0.126797000	F	-8.077525000	-1.710873000	0.116182000
F	-7.647387000	-3.353472000	1.178359000	F	-7.612749000	-3.542796000	1.067443000
F	-7.620605000	-3.663364000	-0.903456000	F	-7.679463000	-3.441127000	-1.032791000
F	7.595713000	3.646773000	0.985122000	F	7.612731000	3.542847000	1.067417000
F	7.681944000	3.369808000	-1.099668000	F	7.679473000	3.441080000	-1.032813000
F	8.074255000	1.744135000	0.192309000	F	8.077523000	1.710881000	0.116243000

Table S9. DFT optimized ground state (S_0) and T_1 state geometry of **2'** in cartesian (XYZ) coordinates

State S_0				**State T_1**			
Pt	3.693251000	-0.352511000	0.000002000	Pt	3.675944000	-0.354329000	-0.000002000
O	3.254083000	-2.296668000	0.000072000	O	3.233146000	-2.301887000	0.000003000
O	5.721213000	-0.761142000	0.000253000	O	5.704646000	-0.759824000	0.000012000
C	1.614407000	1.563431000	-0.000288000	C	1.609506000	1.589485000	-0.000005000
C	1.800874000	0.188303000	-0.000189000	C	1.789842000	0.165126000	-0.000004000
C	0.547085000	-0.440145000	-0.000241000	C	0.557866000	-0.439138000	-0.000001000
C	-0.547084000	0.440144000	-0.000364000	C	-0.557867000	0.439137000	-0.000001000
S	-0.039764000	2.084081000	-0.000456000	S	-0.037607000	2.105650000	-0.000002000
C	-1.800874000	-0.188303000	-0.000398000	C	-1.789842000	-0.165128000	0.000001000
C	-1.614407000	-1.563432000	-0.000313000	C	-1.609507000	-1.589486000	0.000003000
S	0.039764000	-2.084082000	-0.000186000	S	0.037606000	-2.105651000	0.000000000
C	2.782642000	2.381864000	-0.000259000	C	2.764417000	2.385189000	-0.000004000
C	-2.782644000	-2.381863000	-0.000258000	C	-2.764418000	-2.385190000	0.000001000
N	-3.926020000	-1.653845000	-0.000249000	N	-3.921163000	-1.644646000	-0.000002000
C	-5.103798000	-2.263375000	-0.000201000	C	-5.093982000	-2.257593000	-0.000003000
C	-5.253031000	-3.642936000	-0.000157000	C	-5.245284000	-3.637620000	-0.000002000
C	-2.849189000	-3.775058000	-0.000210000	C	-2.841919000	-3.788587000	0.000002000
C	-4.077078000	-4.397925000	-0.000160000	C	-4.064423000	-4.405250000	0.000000000
C	2.849188000	3.775058000	-0.000359000	C	2.841916000	3.788586000	-0.000005000
C	4.077075000	4.397926000	-0.000311000	C	4.064421000	4.405250000	-0.000004000
C	5.253030000	3.642937000	-0.000162000	C	5.245282000	3.637620000	-0.000002000
C	5.103797000	2.263376000	-0.000069000	C	5.093980000	2.257593000	-0.000001000
N	3.926019000	1.653845000	-0.000117000	N	3.921162000	1.644646000	-0.000002000
C	-6.596378000	-4.270947000	-0.000107000	C	-6.586368000	-4.264190000	0.000000000
C	6.596376000	4.270948000	-0.000116000	C	6.586366000	4.264191000	0.000000000
H	-5.980127000	-1.596430000	-0.000186000	H	-5.973313000	-1.594035000	-0.000006000
H	-1.919827000	-4.360231000	-0.000214000	H	-1.913588000	-4.376278000	0.000003000
H	1.919825000	4.360231000	-0.000474000	H	1.913586000	4.376277000	-0.000006000
H	5.980127000	1.596432000	0.000055000	H	5.973312000	1.594036000	0.000000000
Pt	-3.693250000	0.352511000	-0.000279000	Pt	-3.675944000	0.354329000	-0.000003000
O	-5.721212000	0.761141000	0.000134000	O	-5.704646000	0.759826000	-0.000001000
O	-3.254082000	2.296668000	-0.000284000	O	-3.233143000	2.301886000	-0.000004000
C	-4.088325000	3.238379000	0.000675000	C	-4.069294000	3.241279000	0.000002000
C	-5.479309000	3.110909000	0.001527000	C	-5.460482000	3.110701000	0.000007000
C	-6.210346000	1.912913000	0.001025000	C	-6.191653000	1.912950000	0.000004000
C	-3.475039000	4.593742000	0.000243000	C	-3.460265000	4.598492000	0.000002000
C	-7.698323000	1.978941000	0.001588000	C	-7.679326000	1.980149000	0.000011000
C	4.088327000	-3.238379000	0.000436000	C	4.069298000	-3.241279000	0.000002000
C	5.479311000	-3.110910000	0.000742000	C	5.460485000	-3.110699000	0.000005000
C	6.210347000	-1.912914000	0.000593000	C	6.191655000	-1.912948000	0.000010000
C	7.698324000	-1.978941000	0.000854000	C	7.679328000	-1.980144000	0.000014000
C	3.475037000	-4.593741000	0.000406000	C	3.460270000	-4.598493000	-0.000001000
H	-6.057114000	4.042445000	0.002421000	H	-6.039356000	4.041519000	0.000013000
H	-2.826435000	4.707079000	-0.886950000	H	-2.806143000	4.711260000	-0.883121000
H	-2.814635000	4.702510000	0.879193000	H	-2.806115000	4.711248000	0.883106000
H	-4.215425000	5.407395000	0.006897000	H	-4.203049000	5.409920000	0.000019000

H	-8.090377000	3.006924000	0.002597000	H	-8.070879000	3.008258000	0.000017000
H	-8.093314000	1.444650000	0.883888000	H	-8.074544000	1.446472000	0.882558000
H	-8.093904000	1.446194000	-0.881385000	H	-8.074551000	1.446480000	-0.882539000
H	6.057116000	-4.042446000	0.001072000	H	6.039361000	-4.041517000	0.000003000
H	8.093752000	-1.445706000	-0.881891000	H	8.074552000	-1.446461000	-0.882527000
H	8.090379000	-3.006924000	0.001240000	H	8.070883000	-3.008253000	0.000004000
H	8.093467000	-1.445138000	0.883382000	H	8.074546000	-1.446481000	0.882571000
H	2.821799000	-4.705328000	-0.883573000	H	2.806127000	-4.711250000	-0.883109000
H	2.819246000	-4.704249000	0.882616000	H	2.806143000	-4.711261000	0.883118000
H	4.215440000	-5.407405000	0.001894000	H	4.203056000	-5.409920000	-0.000011000
H	-4.132149000	-5.496565000	-0.000122000	H	-4.126186000	-5.503241000	0.000001000
H	4.132146000	5.496565000	-0.000389000	H	4.126182000	5.503241000	-0.000004000
H	-7.400710000	-3.517160000	-0.000114000	H	-7.392148000	-3.511633000	-0.000027000
H	-6.745393000	-4.916300000	0.884933000	H	-6.736523000	-4.912440000	0.884119000
H	-6.745433000	-4.916355000	-0.885101000	H	-6.736504000	-4.912484000	-0.884089000
H	6.745289000	4.916525000	0.884777000	H	6.736514000	4.912453000	0.884111000
H	6.745533000	4.916133000	-0.885256000	H	6.736507000	4.912474000	-0.884096000
H	7.400708000	3.517162000	0.000160000	H	7.392146000	3.511635000	-0.000012000

References.

1. G. Sheldrick, *Acta Cryst. A*, 2015, **71**, 3-8.
2. O. V. Dolomanov, L. J. Bourhis, R. J. Gildea, J. A. K. Howard and H. Puschmann, *J. Appl. Cryst.*, 2009, **42**, 339-341.
3. A. L. Dobryakov, S. A. Kovalenko, A. Weigel, J. L. Pérez-Lustres, J. Lange, A. Müller and N. P. Ernsting, *Rev. Sci. Instrum.*, 2010, **81**, 113106.
4. T. Wilhelm, J. Piel and E. Riedle, *Opt. Lett.*, 1997, **22**, 1494-1496.
5. R.-J. Kutta, T. Langenbacher, U. Kensy and B. Dick, *Appl. Phys. B*, 2013, **111**, 203-216.
6. R.-J. Kutta, U. Kensy and B. Dick, in *Chemical Photocatalysis*, ed. B. König, De Gruyter, Leipzig, 2013, DOI: https://doi.org/10.1002/anie.201307399, pp. 295–318.
7. A. A. Gorman, I. Hamblett, C. Lambert, A. L. Prescott, M. A. J. Rodgers and H. M. Spence, *J. Am. Chem. Soc.*, 1987, **109**, 3091-3097.
8. C. Martí, O. Jürgens, O. Cuenca, M. Casals and S. Nonell, *J. Photochem. Photobiol. A*, 1996, **97**, 11-18.
9. M. J. Frisch, G. W. Trucks, H. B. Schlegel, G. E. Scuseria, M. A. Robb, J. R. Cheeseman, G. Scalmani, V. Barone, B. Mennucci, G. A. Petersson, H. Nakatsuji, M. Caricato, X. Li, H. P. Hratchian, A. F. Izmaylov, J. Bloino, G. Zheng, J. L. Sonnenberg, M. Hada, M. Ehara, K. Toyota, R. Fukuda, J. Hasegawa, M. Ishida, T. Nakajima, Y. Honda, O. Kitao, H. Nakai, T. Vreven, J. A. Montgomery Jr., J. E. Peralta, F. Ogliaro, M. J. Bearpark, J. Heyd, E. N. Brothers, K. N. Kudin, V. N. Staroverov, R. Kobayashi, J. Normand, K. Raghavachari, A. P. Rendell, J. C. Burant, S. S. Iyengar, J. Tomasi, M. Cossi, N. Rega, N. J. Millam, M. Klene, J. E. Knox, J. B. Cross, V. Bakken, C. Adamo, J. Jaramillo, R. Gomperts, R. E. Stratmann, O. Yazyev, A. J. Austin, R. Cammi, C. Pomelli, J. W. Ochterski, R. L. Martin, K. Morokuma, V. G. Zakrzewski, G. A. Voth, P. Salvador, J. J. Dannenberg, S. Dapprich, A. D. Daniels, Ö. Farkas, J. B. Foresman, J. V. Ortiz, J. Cioslowski and D. J. Fox, *Gaussian 09*, Gaussian, Inc., Wallingford, CT, USA, 2009.
10. R. Peverati and D. G. Truhlar, *J. Phys. Chem. Lett.*, 2012, **3**, 117-124.
11. R. Peverati and D. G. Truhlar, *Phys. Chem. Chem. Phys.*, 2012, **14**, 11363-11370.
12. F. Weigend and R. Ahlrichs, *Phys. Chem. Chem. Phys.*, 2005, **7**, 3297-3305.
13. M. Cossi, N. Rega, G. Scalmani and V. Barone, *J. Comput. Chem.*, 2003, **24**, 669-681.